WPEDU-PR(18) 20430

A. F. Mink et al.

Scaling of the toroidal structure and nonlinear dynamics of ELMs on ASDEX Upgrade

Preprint of Paper to be submitted for publication in
Plasma Physics and Controlled Fusion

This work has been carried out within the framework of the EUROfusion Consortium and has received funding from the Euratom research and training programme 2014-2018 under grant agreement No 633053. The views and opinions expressed herein do not necessarily reflect those of the European Commission.

Scaling of the toroidal structure and nonlinear dynamics of ELMs on ASDEX Upgrade

A.F. Mink[1,2], E. Wolfrum[1], M. Dunne[1], M. Hoelzl[1], M. Maraschek[1], R. Fischer[1], M. Cavedon[1], G.F. Harrer[1,3], U. Stroth[1], the ASDEX Upgrade Team

E-mail: felician.mink@ipp.mpg.de
[1]Max-Planck-Institut für Plasmaphysik, Boltzmannstr. 2, 85748 Garching, Germany
[2]Physik Department, E28, TUM, 85748 Garching, Germany
[3]Institute of Applied Physics, TU Wien, Fusion@ÖAW, 1040 Vienna, Austria

April 2018

Abstract. Edge localized modes (ELMs) are magnetohydrodynamic (MHD) instabilities that cause fast periodic relaxations of the strong edge pressure gradient in tokamak fusion plasmas. Magnetic pick-up coils allow the extraction of toroidal mode numbers n during the ELM cycle including the nonlinear crash on ASDEX Upgrade, whereas divertor shunt measurements and the reconstructed equilibrium yield an estimation for ELM duration and losses. This paper investigates how these ELM characterizing parameters change with a variation of plasma parameters.
It is found that the toroidal structure size during the crash is similar to the one existing slightly before and always has a low $n = 1$–7 range. Furthermore, n does not change strongly with most peeling-ballooning relevant parameters such as normalized pressure gradient, bootstrap current density or triangularity, whereas a strong decrease of n with edge safety factor q_{95} is observed in agreement with nonlinear modeling. A simple geometric model is presented, which is capable of explaining the q scaling by existence of ballooned structures that minimize n. Furthermore, the duration of the ELM decreases with q_{95}, whereas the ELM energy losses scale with pedestal energy.

1. Introduction

Edge localized modes (ELMs) are periodically appearing instabilities that cause fast relaxations of the strong edge pressure gradient in the high-confinement regime (H-mode) of tokamak fusion plasmas [1, 2, 3]. These crashes induce strong heat and particle losses and thereby create intense heat fluxes onto the divertor tiles. This can be a major concern for future fusion devices like ITER [4, 5].
The onset criteria of ELMs are typically described by the linear peeling-ballooning boundary in the framework of ideal magnetohydrodynamics (MHD) [6, 7, 8]. However, linear models can only determine whether a certain mode is unstable and thereby potentially grows, whereas obtaining predictions or explanations for details of the ELM

cycle including the fast crash behavior is not possible. Only nonlinear MHD theory can explain the whole dynamics including the coupling of modes, which is thought to be responsible for the fast crash [9]. Furthermore, several other ingredients like the shear flow or the resistivity might play important roles as well during the whole ELM cycle [10, 11, 12].

In order to understand the ELM dynamics it is necessary to check the validity of the (potentially predictive) ELM models. This can be achieved by comparing modeling output to experimental results. One essential parameter for such a comparison is the structure of the ELM crash, which is why it is the subject of investigation with various techniques [13, 14, 15]. Here, the toroidal mode number n is of a special interest [16, 17, 18] because it provides a good comparability to nonlinear 3D MHD codes such as M3D, NIMROD or JOREK as they also use a decomposition in toroidal finite Fourier series [19, 20, 21]. Further parameters that have been investigated are ELM duration and energy or particle losses [22, 23]. In addition to the parameters of the crash, also the structure of ELM-preceding fluctuations have been investigated and similarity to the crash structure itself was stated [24, 25]. However, it is not yet clear how these ELM precursing fluctuations are connected to the crash, which is also often not accessible to nonlinear modelling if initiated from already ELM unstable equilibria.

Recent quantitative comparisons of n and other parameters of the ELM crash between the nonlinear code JOREK and results obtained on the ASDEX Upgrade tokamak demonstrated the progress in understanding the ELM crash by nonlinear modeling [26]. The consequent next step is to investigate how the mode numbers change with critical parameters. In this paper we therefore introduce a database of 30 shots containing more than 2500 type-I ELM crashes on the ASDEX Upgrade tokamak and investigate how the structure size and various other parameters change with plasma parameters, which enables a more detailed testing of the codes in the future. The main focus here is on changing the peeling-ballooning relevant parameters such as normalized pressure gradient, bootstrap current density, triangularity or magnetic shear and investigate their effect on the ELM precursor and crash parameters, i.e. toroidal mode number and ELM duration and losses. Section 2 presents the parameters and their range included in the database and how the ELM crash mode numbers are evaluated. Section 3 shows the results of the parameter scaling, which are then discussed in section 4 and summarized in section 5.

2. Methods

Edge localized modes appear as strong bursts in magnetic pick-up coils and other plasma diagnostics. Figure 1 (a) shows a spectrum of three ELM cycles obtained from a magnetic pick-up coil measuring radial magnetic fluctuations at the low field side (LFS) midplane of the ASDEX Upgrade tokamak. During the ELM crash a broad spread in frequency is observed but low frequencies $f \leq 25\,\mathrm{kHz}$ (marked with black boxes) are dominant. Furthermore, modes in a high frequency range $f \geq 200\,\mathrm{kHz}$ (marked with red

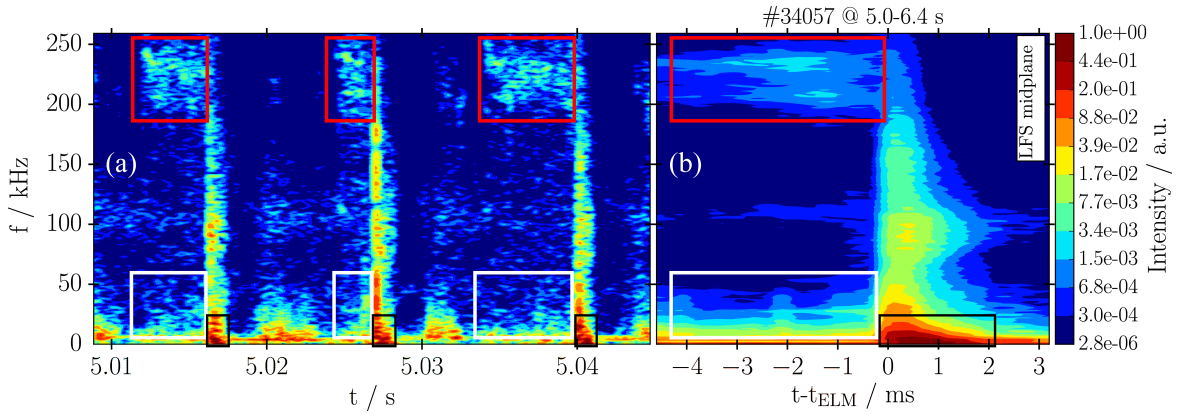

Figure 1. (a) Spectrum obtained from a LFS midplane coil measuring radial magnetic fluctuations during three ELM cycles and (b) spectrum averaged over 100 ELMs synchronized to their onset at $t - t_{\mathrm{ELM}} = 0$. Red and white boxes mark high ≥ 180 and low $\leq 75\,\mathrm{kHz}$ frequency fluctuations during the cycle, whereas black boxes mark the intense low frequency fluctuations during the crash.

boxes) appear in between the crashes. These modes appear when the pedestal gradients are clamped, but are not thought to be directly connected to the crash itself [27]. In addition to that, modes appear in a frequency range $f = 0$–$75\,\mathrm{kHz}$ (marked with white boxes) during the ELM cycle. As in some cases their amplitude increases significantly just before the ELM crash and their structure is similar to the one observed during the crash, they are considered as ELM precursors [25, 28]. These precursing modes are well separated from high frequency modes in frequency (as they have $f \leq 150\,\mathrm{kHz}$) and usually also in rotation velocity [24].

Figure 1 (b) shows a spectrum obtained from the same LFS midplane coil, but averaged over and synchronized to all 100 ELM onsets at $t - t_{\mathrm{ELM}} = 0$ within a phase of constant plasma parameters. Again the same modes as in the spectrum of the three ELM cycles are visible. Such an ELM synchronization is especially helpful when determining toroidal mode numbers of pre-ELM and ELM crash modes as explained in Ref. [24]. Furthermore, as the described modes do not appear with single mode numbers but ensembles of several structures, it is necessary to introduce a quantitative measure which can be compared for the different mode number distributions during ELM cycles of various discharges. Therefore, a mean and standard deviation was introduced. Figure 2 gives the results of both quantities evaluated during the ELM crash for two representative discharge time traces. The figure shows two mode number spectra evaluated from 50 ELM crashes of both discharges (a,b). These spectra are obtained during a 2 ms long window around 1 ms after the ELM onset, in line with the ELM duration of about 2 ms. The two discharges have a different q_{95} of (a) 3.1 and (b) 6.9. The ELM crash is dominated by different mode numbers, i.e. $n = 2$–7 for the low and $n = 1$–6 for the high q_{95} discharge, which appear in the previously mentioned typical crash frequency range below 25 kHz. The bottom plot (c) shows the mode number distribution obtained by integrating the mode number spectra of both discharges (a,b) over the frequency. Also shown are

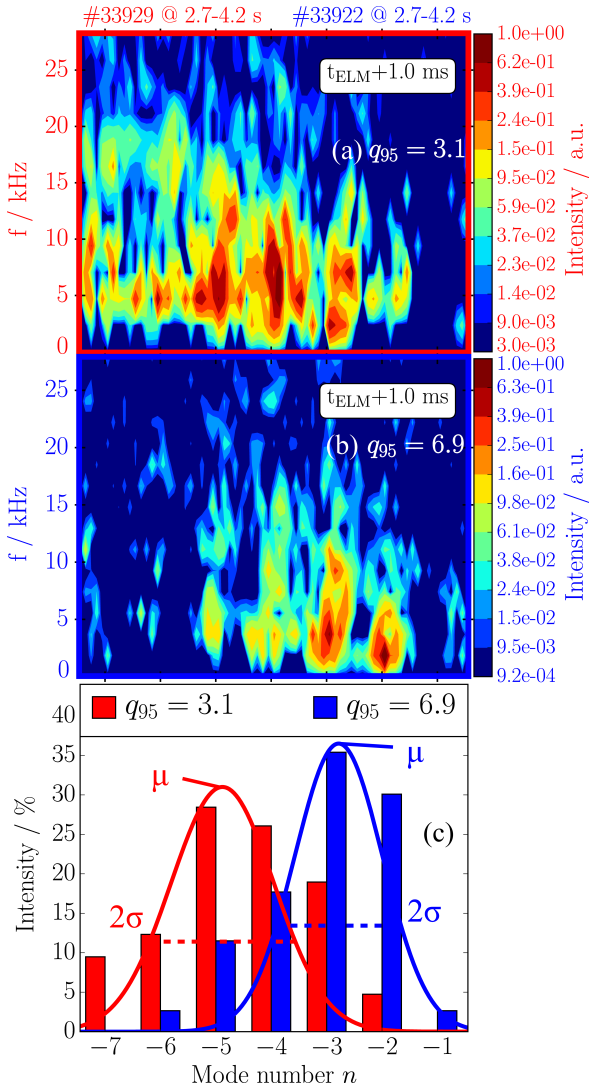

Figure 2. (a,b) Toroidal mode number n spectra of the ELM crash for two discharges with different q_{95}, obtained from a 2 ms time window around 1 ms after 50 ELM crash onsets. (c) The integrated n distributions, which can be described by mean μ and standard deviation σ, according to the fitted Gaussian curves.

two Gaussian distributions defined from the mean μ and the standard deviation σ of the distributions. Although mode numbers are not necessarily following a Gaussian distribution, both parameters form a quantitative measure for describing the difference in mode numbers. Therefore, an average toroidal mode number and its spread, that are used in the following, are defined as $\langle n \rangle = \mu \pm \sigma$. In the here shown cases this yields $\langle n \rangle = 4.5 \pm 1.3$ and 3.1 ± 1.1 for the low and high q_{95} case.

Similarly to the here defined average toroidal structure of the crash, also the average toroidal structure of the precursing modes $f \leq 150\,\mathrm{kHz}$ that appear before the crash can be defined from mean and standard deviation. Other parameters of the ELM that are investigated in the following are the ELM duration and energy losses. The duration is defined from divertor shunt current measurements, which are a proxy for the transport

Table 1. ELM and plasma parameters and their range investigated in the database. The ranges of τ_{Div}, ΔW_{MHD} and $\Delta W^{\mathrm{rel}}_{\mathrm{MHD}}$ exclude the highest and lowest 1 % of the data as these quantities contain few strong outliers.

ELM Parameter	Formula	Range
Average ELM crash toroidal mode number	$\langle n \rangle_{\mathrm{ELM}}$	1.9–5.0
Average pre-ELM toroidal mode number	$\langle n \rangle_{\mathrm{PRE}}$	1.8–6.2
ELM duration (in divertor)	τ_{Div}	1.6–5.8 ms
Absolute plasma energy losses	ΔW_{MHD}	10–70 kJ
Relative plasma energy losses	$\Delta W^{\mathrm{rel}}_{\mathrm{MHD}} = \frac{\Delta W_{\mathrm{MHD}}}{W_{\mathrm{MHD}}}$	2–15 %
Plasma Parameter	**Formula**	**Range**
Pedestal top density	n_e	$2.0\text{–}7.5{\cdot}10^{19}\mathrm{m}^{-3}$
Pedestal top temperature	T_e	230–650 eV
Maximum pressure gradient	∇p_e	100–350 kPa/m
Maximum normalized pressure gradient	$\alpha = -\nabla p \frac{2\mu_0 R_0 q^2}{B^2}$	2.0–8.5
Plasma current	I_p	0.6–1.1 MA
Toroidal magnetic field	B_t	1.8–3.0 T
Maximum bootstrap current density [29]	j_{BS}	$0.1\text{–}1.0\,\mathrm{MA/m}^2$
Edge safety factor	q_{95}	2.94–8.07
Safety factor gradient (at $\rho = 0.975$)	∇q	$40\text{–}120\,\mathrm{m}^{-1}$
Normalized magnetic shear (at $\rho = 0.975$)	$s = \frac{r}{q}\frac{\mathrm{d}q}{\mathrm{d}r}$	5.6–6.6
Average triangularity	$\delta = (\delta_{up} + \delta_{low})/2$	0.2–0.4

across the separatrix. It is calculated from the time that the shunt signal stays above a certain threshold value. The ELM losses are obtained from the equilibrium. In total five ELM parameters were investigated within the parameter database in a broad range given in table 1.

From the very basic peeling-ballooning theory it is expected that the ELM is driven by edge current density and pressure gradient. Both parameters can cause modes to become unstable and the structure of the modes is thought to shrink in size (increase in n) and is more poloidally asymmetric if it is more pressure than current driven [30]. Furthermore, both types of modes, i.e. high n pressure driven and low n current driven, are also stabilized by parameters like the magnetic shear s. Moreover, edge current density cannot be independent from the pressure gradient due to the neoclassical bootstrap current [29]. This complexity makes it difficult to predict an easy rule of thumb stating for example that increasing the pressure gradient should increase mode numbers during the crash. Only nonlinear modeling can give conclusive results on how mode numbers change with plasma parameters, but this is computationally expensive. Therefore, discharges were performed in a wide parameter range in order to investigate their influence on the structure and other properties of the ELM crash. This database can then be used as a look up table for future comparisons to modeling in order to

Table 2. Pearson correlation matrix with correlation coefficients c_P of the investigated plasma and ELM parameters presented in table 1

Parameters	n_e	T_e	∇p	α	I_p	B_t	j_{BS}	q_{95}	∇q	s	δ	$\langle n\rangle_{\mathrm{ELM}}$	$\langle n\rangle_{\mathrm{PRE}}$	τ_{Div}	ΔW_{MHD}	$\Delta W^{\mathrm{rel}}_{\mathrm{MHD}}$
n_e	1.00	0.05	0.62	-0.39	0.91	-0.61	0.29	-0.94	-0.94	0.31	-0.22	0.85	0.64	-0.46	0.46	-0.34
T_e	0.05	1.00	0.63	0.65	0.03	0.07	0.85	-0.09	-0.05	-0.20	0.40	-0.05	0.02	-0.22	0.32	-0.29
∇p	0.62	0.63	1.00	0.34	0.63	-0.35	0.78	-0.67	-0.61	0.08	0.10	0.48	0.26	-0.48	0.63	-0.41
α	-0.39	0.65	0.34	1.00	-0.47	0.18	0.64	0.41	0.47	-0.21	0.57	-0.52	-0.34	0.11	0.08	-0.06
I_p	0.91	0.03	0.63	-0.47	1.00	-0.42	0.25	-0.92	-0.95	0.11	-0.32	0.83	0.58	-0.56	0.60	-0.26
B_t	-0.61	0.07	-0.35	0.18	-0.42	1.00	-0.13	0.64	0.60	-0.51	0.13	-0.64	-0.56	0.37	-0.29	0.21
j_{BS}	0.29	0.85	0.78	0.64	0.25	-0.13	1.00	-0.27	-0.24	-0.11	0.55	0.03	0.19	-0.33	0.63	-0.14
q_{95}	-0.94	-0.09	-0.67	0.41	-0.92	0.64	-0.27	1.00	0.98	-0.37	0.30	-0.89	-0.61	0.53	-0.52	0.39
∇q	-0.94	-0.05	-0.61	0.47	-0.95	0.60	-0.24	0.98	1.00	-0.22	0.29	-0.90	-0.63	0.60	-0.52	0.28
s	0.31	-0.20	0.08	-0.21	0.11	-0.51	-0.11	-0.37	-0.22	1.00	-0.14	0.27	0.13	0.26	0.05	-0.21
δ	-0.22	0.40	0.10	0.57	-0.32	0.13	0.55	0.30	0.29	-0.14	1.00	-0.47	-0.09	0.13	0.17	0.12
$\langle n\rangle_{\mathrm{ELM}}$	0.85	-0.05	0.48	-0.52	0.83	-0.64	0.03	-0.89	-0.90	0.27	-0.47	1.00	0.62	-0.48	0.36	-0.32
$\langle n\rangle_{\mathrm{PRE}}$	0.64	0.02	0.26	-0.34	0.58	-0.56	0.19	-0.61	-0.63	0.13	-0.09	0.62	1.00	-0.30	0.32	-0.15
τ_{Div}	-0.46	-0.22	-0.48	0.11	-0.56	0.37	-0.33	0.53	0.60	0.26	0.13	-0.48	-0.30	1.00	-0.25	0.26
ΔW_{MHD}	0.46	0.32	0.63	0.08	0.60	-0.29	0.63	-0.52	-0.52	0.05	0.17	0.36	0.32	-0.25	1.00	0.17
$\Delta W^{\mathrm{rel}}_{\mathrm{MHD}}$	-0.34	-0.29	-0.41	-0.06	-0.26	0.21	-0.14	0.39	0.28	-0.21	0.12	-0.32	-0.15	0.26	0.17	1.00

better understand the ELM. The plasma parameters and their range investigated in the database are given in table 1. The equilibrium quantities such as B, I, q or δ are obtained from one single time point just before the crash, whereas profile quantities such as n_e, T_e or j_{BS} are obtained from averaging data over short time ranges before the ELM onset during which the profiles are clamped. All of the here discussed plasma parameters play a role in basic linear MHD theory either by driving or stabilizing current or pressure driven modes. These effects will be discussed shortly in the following. However, the main result of the database will be that these linear theoretical tendencies cannot describe the observed trends in the ELM crash.

Density and temperature profiles are responsible for the pressure profile, whose edge gradient drives the ballooning modes. Plasma current and toroidal magnetic field produce the confinement via $\nabla p = \vec{j} \times \vec{B}$. However, current also drives the current instabilities, so does the bootstrap current density, which is mainly proportional to the pressure gradient. The edge safety factor is not directly linked to the peeling-ballooning model, but it is a proxy for its gradient. The gradient and the normalized gradient of edge safety factor, i.e. the shear s, stabilize especially ballooning modes. The shear, however, is locally modified by the bootstrap current. The triangularity δ increases stability of ballooning modes, which is due to the fact that the bad curvature region is reduced on a flux surface. This allows higher pressure gradients and the concomitant stronger bootstrap currents can modify the magnetic shear and allow access to the second stability regime [31].

3. Results

All of the previously mentioned parameters were tested on their correlation with each other setting up a matrix, see table 2, of linear Pearson correlation coefficients

$c_P \in [-1, 1]$ for the given 30 discharges. In the following we discuss the results of these correlations and dependencies beginning with the toroidal mode number as the MHD relevant parameter, whereas the transport characterizing parameters like duration and energy losses are discussed afterwards.

As mentioned before, the crash is dominated by a low n structure. Furthermore, the structure of the fluctuations that appear in a medium frequency range $f \leq 150\,\mathrm{kHz}$ before the crash scales with the ELM crash structure. The correlation coefficient of these average structures appearing before and during the ELM crash, $\langle n \rangle_{\mathrm{PRE}}$ and $\langle n \rangle_{\mathrm{ELM}}$, is $c_P = 0.62$, indicating a positive correlation. Figure 3 shows both quantities plotted against the each other for the 30 evaluated H-mode discharges. Additionally, the bisecting line is plotted in green, indicating the points where $\langle n \rangle_{\mathrm{PRE}} = \langle n \rangle_{\mathrm{ELM}}$. From this plot it might be concluded that precursing modes just before the crash have similar toroidal structure as the crash itself. It is not necessarily true that structures before and during the crash are exactly the same as some of the discharges show deviations from the bisecting line even within their spread, i.e. precursing modes tend to have slightly higher $\langle n \rangle$ values. Nevertheless, higher $\langle n \rangle_{\mathrm{PRE}}$ also show higher $\langle n \rangle_{\mathrm{ELM}}$ and low $\langle n \rangle$ accordingly. Furthermore, it can be concluded that there are no cases where precursing medium frequency modes have high mode numbers like the quasi saturated high frequency oscillations of the ELM cycle with $n \approx 10$. Similarly, also the crash does not have such high mode numbers even in a very broad parameter range of ASDEX Upgrade discharges. This fits to the results obtained previously [26], that the ELM crash is a result of nonlinear coupling yielding low n modes. Furthermore, the similarity of structures before and during the crash points in the direction that the mechanism that determines their n is similar, which raises the question whether the structure before the crash might even influence the ELM crash structure.

As the n appearing before and during the ELM are always in a similar range and scale similarly with the investigated parameters, it is enough to include only one of them in the following discussion. From the Pearson matrix it can be seen that the correlation coefficients $\langle n \rangle_{\mathrm{ELM}}$ and $\langle n \rangle_{\mathrm{PRE}}$ have the same tendencies, but the ones for $\langle n \rangle_{\mathrm{ELM}}$ have higher values if a clear trend is observable. Therefore, only the $\langle n \rangle_{\mathrm{ELM}}$ are included in the following discussion and the index is omitted for readability ($\langle n \rangle_{\mathrm{ELM}} = \langle n \rangle$). However, similar conclusions as for the $\langle n \rangle$ during the crash can be drawn for the precursing $\langle n \rangle_{\mathrm{PRE}}$.

The strongest correlation of $c_P = -0.9$ of $\langle n \rangle$ is found for the gradient of the safety factor ∇q in the pedestal, which is also strongly correlated with the edge safety factor q_{95} itself ($c_P = 0.98$). This linear dependence of the toroidal structure $\langle n \rangle$ on q_{95} is also shown in Figure 4 (a). From basic ballooning theory it would be expected that the normalized magnetic shear $s = \frac{r}{q}\frac{dq}{dr}$ is stabilizing ballooning modes and would therefore cause smaller peeling n during the ELM crash. However, from the experimental investigation shown in Figure 4 (b) no clear trend can be observed for s. Though it has to be pointed out that the shear in general is not at all easy to quantify, as also very local variations might change effects on the ELM crash strongly. Such local variations of the shear can

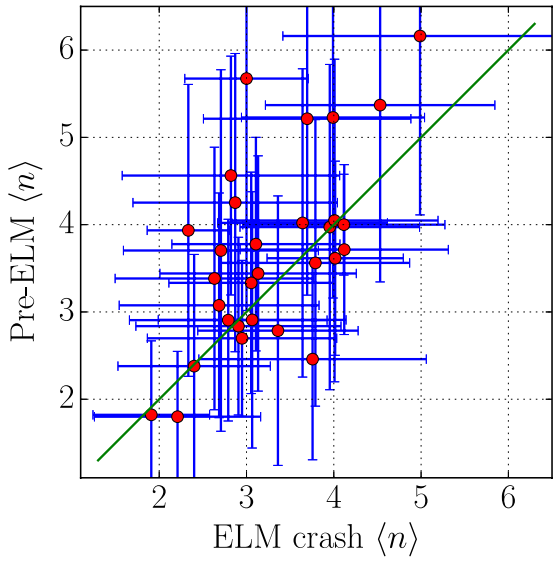

Figure 3. Average toroidal mode numbers $\langle n \rangle$ of mode structures before ELM crash and during the crash. The bisecting line indicating $\langle n \rangle_{\mathrm{PRE}} = \langle n \rangle_{\mathrm{ELM}}$ is plotted in green.

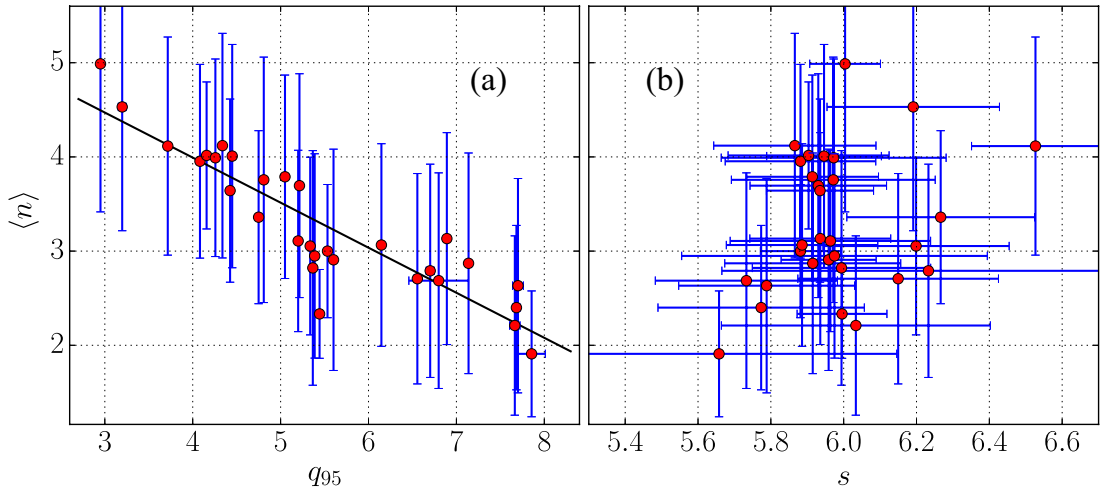

Figure 4. Average toroidal mode numbers $\langle n \rangle$ of mode structures during the crash against (a) edge safety factor q_{95} and (b) normalized magnetic shear s in the pedestal.

be induced for example by the peaking of the bootstrap current near the edge which was not taken into account for the equilibrium and thereby s determination. Instead the shear used in this database is taken from the pedestal top as a rough proxy for the global shear throughout the pedestal region. This is maybe also the reason why the shear variation in this data base is just about 10 % and no clear trend for $\langle n \rangle$ can be observed.

As the edge safety factor is mainly determined by plasma current and toroidal magnetic field the question arises whether also one of these parameters could be responsible for determining $\langle n \rangle$. The correlation coefficients suggest a linear dependence of $\langle n \rangle$ on

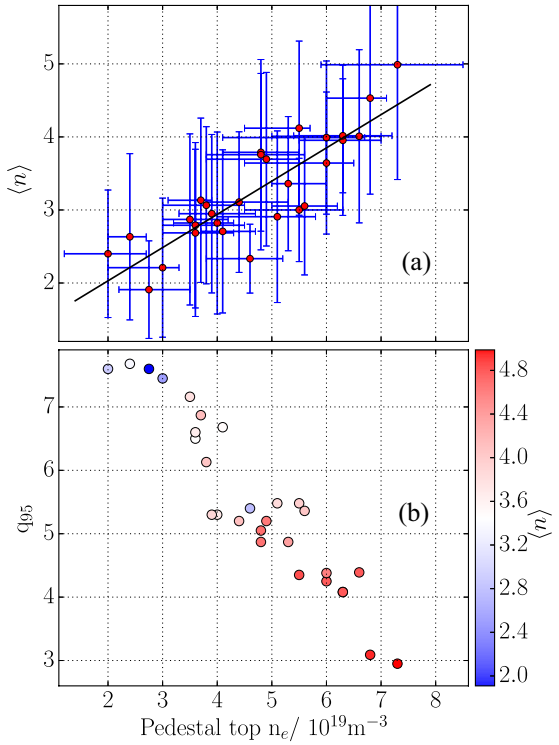

Figure 5. Averaged toroidal mode number dependence on (a) density alone and (b) together with q_{95}, where the blue to red color range stands for low to high n.

the plasma current, which is strongly coupled to pedestal top density n_e in this set of discharges. The increase of $\langle n \rangle$ with pedestal top density n_e is shown in figure 5 (a). Furthermore, figure 5 (b) shows q_{95} against the density with $\langle n \rangle$ color coded, going from blue to red with increasing average mode number. From the previous plots and the relations shown here it is not clear whether it is q_{95} or density and thereby the current that is influencing $\langle n \rangle$. There are discharge pairs with similar q_{95} but varying $\langle n \rangle$ as well as with similar density n_e and varying $\langle n \rangle$. Dedicated experiments would therefore be necessary in order to scan q_{95} with the magnetic field B_t and not via the current. This might disentangle the influence of q_{95} and n_e on the crash structure. However, a similar investigation on the structure of the ELM crash with fast camera imaging on DIII-D also found an increase of n with pedestal density [17]. The effect of the edge safety factor was not investigated there.

Other parameters in this database that are thought to influence the $\langle n \rangle$ values according to basic peeling ballooning theory seem to play either a minor role or influence the crash either nonlinearly or in a manifold way, making a plain linear correlation analysis useless. Two examples for parameters with such a behavior are the normalized pressure gradient and triangularity. Figure 6 (a) shows $\langle n \rangle$ against the maximum normalized pressure gradient $\alpha_{\max}$. As pointed out before the ballooning part should play a bigger role if the gradient is increased. On the other hand also the bootstrap current j_{BS} increases making the peeling modes more unstable. At the same time the j_{BS} peak changes the local shear giving access to the second stability regime of ballooning modes

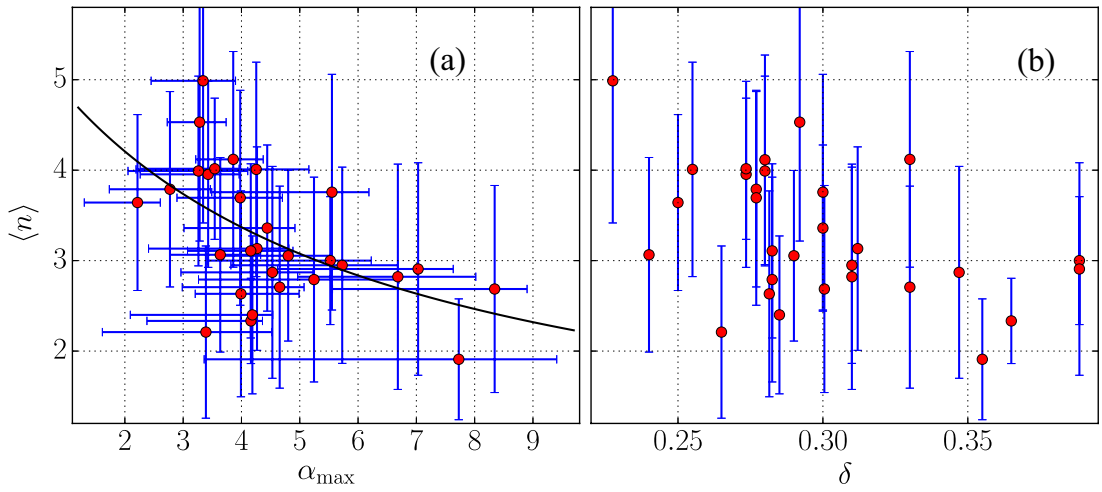

Figure 6. Average toroidal mode numbers $\langle n \rangle$ of mode structures during the crash against (a) the normalized pressure maximum gradient α together with a $1/\alpha$-fit to guide the eye and against (b) the average triangularity δ.

[32]. It is therefore not straight forward to state which n are expected. The experimental evaluation, however, shows a slight tendency towards lower mode numbers for higher normalized pressure gradient α. The line fitted into the data has a $1/\alpha$-dependence which follows this tendency.

Figure 6 (b) shows $\langle n \rangle$ against the average triangularity δ obtained from the plasma equilibrium. As pointed out before δ should stabilize ballooning modes and should therefore lower n [31]. However, from the experimental data investigated here no clear trend can be found, which is also reflected by a smaller correlation of $c_P = -0.47$.

As a last correlation with $\langle n \rangle$ the parameter space of maximum electron pressure gradient ∇p and bootstrap current density j_{BS} was investigated simultaneously. The correlation matrix suggests that there exists no correlation of j_{BS} with the toroidal structure $\langle n \rangle$. Nevertheless, effects might overlap and thereby the real influence of j_{BS} on the structure might be hidden. Figure 7 shows the bootstrap current density j_{BS} and the absolute maximum electron pressure gradient ∇p_e with $\langle n \rangle$ color coded. First of all higher pressure gradients cause higher bootstrap current densities. Secondly, the pressure gradient shows a slightly positive correlation with $\langle n \rangle$, which is in line with the increase of $\langle n \rangle$ with pedestal top electron density (and reduction of q_{95}). However, bluish points with low $\langle n \rangle$ are tending to be more in the upper part of figure 7, whereas reddish points are in the lower, as suggested by the dashed lines that guide the eye. From there it could be stated that bootstrap current indeed reduces $\langle n \rangle$ slightly but as higher bootstrap current is connected with higher pressure gradient, the density (or q_{95}) effect overlaps with it.

Up to now only the effects of parameters on the dominant toroidal mode numbers $\langle n \rangle$ were investigated. In the following the plasma performance affecting parameters like duration and energy losses are discussed.

As the heat load of the ELM on the divertor plates might be a critical issue for future

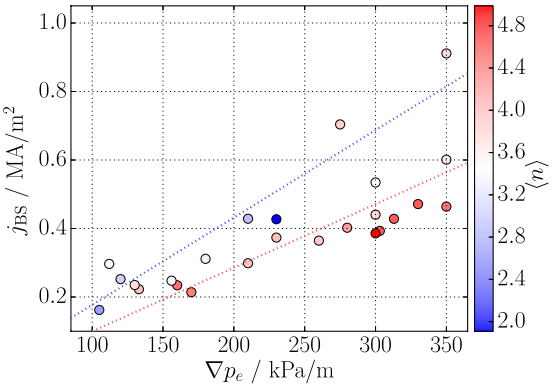

Figure 7. Bootstrap current density maximum j_{BS} against the pressure gradient maximum ∇p. Color coded are from blue to red the average $\langle n \rangle$ during the ELM crash.

fusion devices, it is of high interest to characterize the ELMs in terms of energy losses and duration. The obtained database delivers a big variation of plasma parameters on AUG and can also be used to investigate what influences these ELM losses.

The correlation coefficients for the absolute ELM energy losses ΔW_{MHD} suggest that the losses scale with the pedestal parameters such as density, temperature, pressure gradient and also with plasma current. On the other hand they inversely scale with toroidal magnetic field, ∇q and thereby q_{95}. The duration τ_{Div} and the relative ELM losses ΔW_{MHD} basically scale the other way round. They decrease with pedestal parameters and increases with safety factor. However, correlation coefficients are in some cases very weak, which is maybe due to the fact that these parameters characterizing the losses vary strongly from ELM to ELM even within a phase of constant global plasma parameters.

Figure 8 shows how (a) the ELM duration τ, (b) the ELM induced energy losses ΔW_{MHD} and (c) the relative energy losses scale with edge safety factor q_{95} as one exemplary scaling parameter for the investigated 30 discharges. Shown are the data for all ELMs (black) together with the mean and standard deviation for the 30 discharges. Showing only the mean values and standard deviation is not sufficient here, as the data for ELM duration and losses in some cases do not at all follow Gaussian distributions within a discharge. For example there can be discharges containing a group of very short ELMs and a group of very long ELMs, which was also seen in similar investigations on the JET tokamak [23]. This points towards another hidden parameter, which is changing from ELM to ELM within a discharge, but cannot be revealed by this database. From the data in (a) and (b), however, it can be seen that there is a clear scaling with q_{95}, in a way that it sets an upper boundary for ELM duration and losses, indicated by the black dashed lines. At high q_{95} the ELM duration covers a wide range up to 7 ms, but ELM crashes tend to appear with lower losses. Conversely, at low q_{95} the losses can cover a wide range but then the duration is very limited. Figure 8 (c), however, shows that the relative energy losses seem to be almost independent of the edge safety factor.

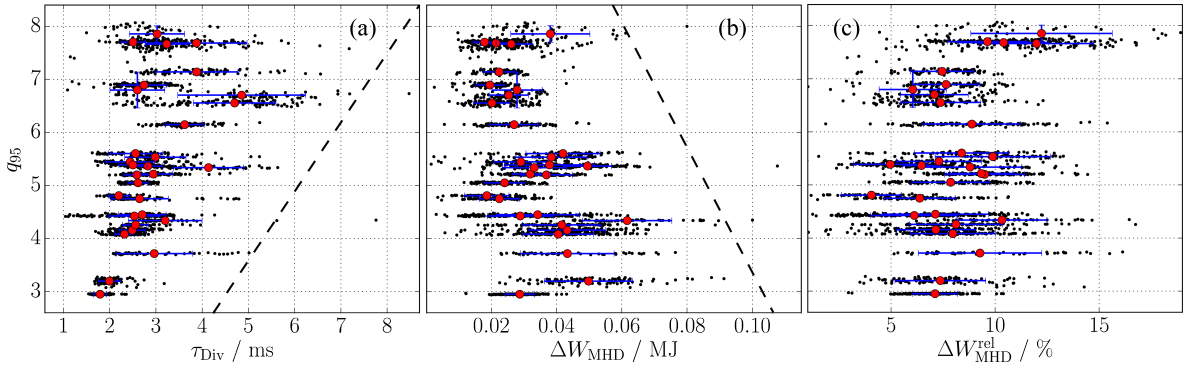

Figure 8. Edge safety factor q_{95} against (a) the duration, (b) the absolute ELM energy losses and (c) the relative energy losses of all 2500 ELMs together with the mean and standard deviations of the 30 discharges. Black dashed lines mark the parameter space beyond which almost none of the ELMs appear.

Only highest q_{95} seem to cause ELMs with slightly higher relative losses of 10–15%.

4. Discussion

Previously mentioned investigations on JET [23] found that the ELM length scales inversely with the pedestal parameters, namely the pedestal energy. Furthermore, investigations on different machines found that the peak energy fluence, which is comparable to the here defined energy losses, scaled with pedestal density and temperature [33]. Both findings fit to the here found scaling with q_{95} as the low q_{95} discharges have usually higher pedestal top pressures.

An explanation why the transport events are shorter or longer was not found in previous publications. Therefore, the finding that the edge safety factor might play a major role, is another step forward in understanding the ELM. From this observation one possible explanation for the ELM length could be that ELMs of high q_{95} plasmas just influence broader regions of the plasma. This would also be in line with the fact that a strong ∇q reduces $\langle n \rangle$ and thereby broadens the structure size, as seen in the previous section. This influence of broader regions of the ELM with higher edge safety factor is also experimentally observed in the propagation distance of cold pulses which are induced by ELM crashes [34].

Another approach for explaining the ELM duration could be drawn from the pedestal parameters directly, namely ∇p. Previous studies showed that the radial electric field being responsible for the edge poloidal rotation and thereby the edge transport barrier in H-Mode is mainly neoclassically driven and therefore proportional to the ion pressure gradient divided by density $\nabla p_i / n_e$ [35]. Furthermore, a certain radial electric field larger than about 15 kV/m at $|B_t| = 2.5$ T is needed in order to maintain the H-mode in ASDEX Upgrade [36]. Recent findings showed that the radial electric field drops down to similar values and below during the ELM crash [37]. From there the speculative hypothesis is that the crash length is due to the plasma going into L-mode, during

which the transport is high, and taking several milliseconds until going back to H-mode by restoring ∇p_i and thereby electric field and edge rotation. In this case it would depend on the ion dynamics how fast the edge transport barrier can be restored and the ELM ends.

In order to clarify whether the mode structure or the pedestal parameters determine the ELM duration, further investigations taking into account also the ion pressure gradient are needed. In our database the relative ELM energy losses are mostly between 4–13 % and do not show significant dependencies.

Summarizing the obtained results for the structure of the ELM crash yields that the peeling-ballooning relevant parameters such as α, s, δ or j_{BS} barely influence the structure of the ELM crash. However, the result that $\langle n \rangle$ varies strongly with edge safety factor and ∇q is very robust. In the following an intuitive geometrical explanation for this behavior is given. The basic idea of the model is that the ELM crash as a mixture of peeling and ballooning modes is driven nonlinearly in the whole region of the pedestal gradients trying to maximize structure size (minimize n), but a low ∇q hampers the existence of low n structures due to larger separation of interfering modes on rational surfaces.

Figure 9 visualizes the effect of edge safety factor and magnetic shear on mode structures. The bottom plots show realistic artificial q profiles and according ∇q and s profiles in arbitrary units. The two types of profiles visualized here have (a,b) low $q_{95} = 3.2$ and (d,e) high $q_{95} = 7.0$, similar to the experimental cases shown in figure 2. From the bottom plots it can be seen that the s parameter does not vary a lot although q and ∇q are about doubled, similar as in the previously presented data set. The top plots show compositions A^i of artificial mode structures in the $\theta^*/\psi_{\mathrm{N}}$ plane of the edge region, which are described by:

$$A^i\left(\psi_{\mathrm{N}}, \theta^*\right) = \exp\left(-\left(\frac{\psi_{\mathrm{N}} - \overline{\psi}^i_{\mathrm{N}}}{\Omega}\right)^2\right) \sin\left(m^i \theta^*\right), \tag{1}$$

with the straight field line coordinate θ^* and the normalized poloidal flux ψ_{N}. Each composition consists of three modes with width Ω on rational surfaces $q(\psi_{\mathrm{N}}) = m/n$ with one n but different m^i values, given at the top of the plots. The different central positions of the mode compositions $\overline{\psi}_{\mathrm{N}}$ are sketched with black dashed lines in the profile plots.

Ballooning modes can be interpreted as an overlap of several close-by mode structures that interfere such that they have an increased amplitude in the bad curvature region ($\theta^* = 0$). Figure 9 (a) shows a composition of such modes with $n = 2$ at the $q = 4, 4.5$ and 5 surface ‡. Due to the low q shear they are too far apart in order to interact properly. Therefore, it is unlikely that such a low n composition exists in this region for a low q profile as it can not sufficiently incorporate the ballooning drive. The first idea of the geometrical model is therefore that the modes need to be close enough to

‡ In this region there are no closer rational surfaces for $n = 2$ as Δm of the modes cannot be smaller than $\Delta m = 1$.

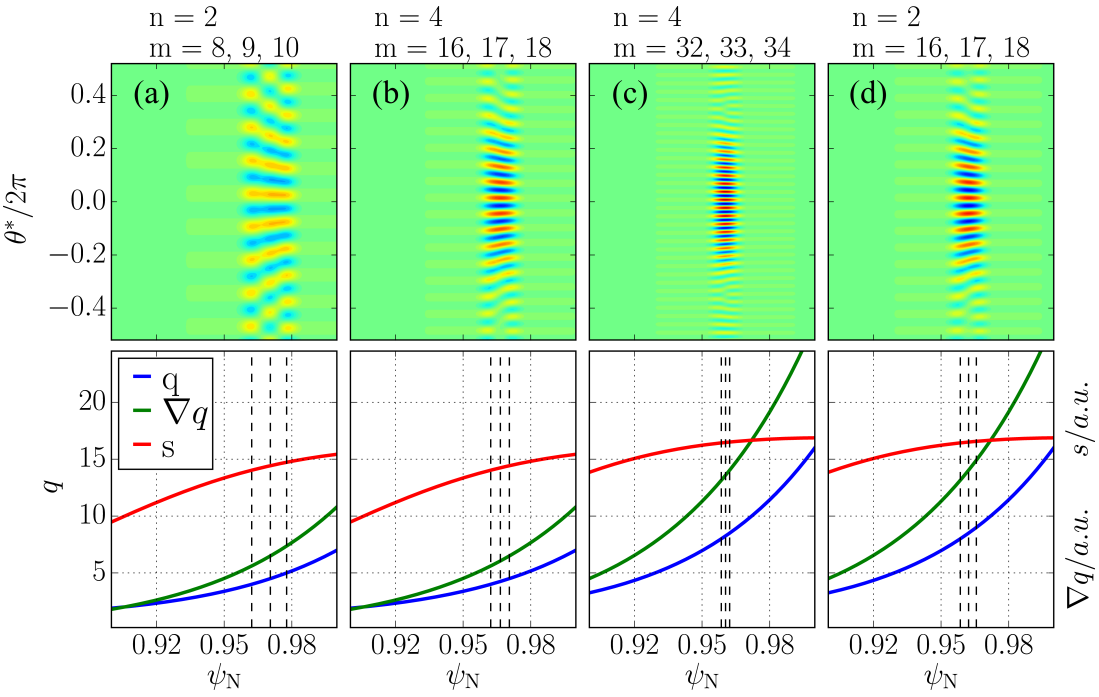

Figure 9. (Top) Artificial mode structures in the θ^*/ψ_N plane for (bottom) two different q, ∇q and s profiles: (a,b) weak shear with $q_{95} = 3.2$ and (c,d) stronger shear with $q_{95} = 7.0$.

interfere. Figure 9 (b) shows $n = 4$ modes, which lead to a ballooned structure in the LFS region. The interaction of modes is possible because the rational surfaces are close enough together at $q = 4, 4.25$ and 4.5. Figure 9 (c) also shows $n = 4$ modes but in the steeper q profile. The modes in the same plasma region now have higher q values of $q = 8, 8.25$ and 8.5 and are closer together as also ∇q is higher, which leads to narrower ballooning modes. However, with the steeper q profile also $n = 2$ modes, figure 9 (d), can be close enough to interfere at $q = 8, 8.5$ and 9.0. From there it is clear that there are two possibilities in order to obtain ballooned modes. Either n or ∇q is high enough. However, the experiments showed that no high $n \geq 10$ appeared at all during the ELM crash. Similarly, also nonlinear modeling showed that modes couple to form low $nn = 1$–5 structures [9, 26]. From this observation it seems that the ELM crash modes are most unstable with minimized n, meaning larger structures. In the context of plasma turbulence this effect of a transition to larger structure sizes is known as inverse cascading [38, 39, 40]. In the frame of MHD this is explained by the mode minimizing the energy of the system by influencing the broadest possible region of the pedestal gradients. Assuming now that the crash modes show such an inverse cascading and minimize n, the mode in figure 9 (d) would not exist, because also the $n = 2$ components are close enough to interact within the steep q profile, but have lower n. This is exactly what is seen in the experiment. If q_{95} and thereby ∇q is high, lower n are observed, whereas higher n are found at low q_{95}. This concept of minimizing n can also be formulated such that the ELM crash modes always show up with the same dominant

m structures regardless of the q profile, which is exactly the case in figures 9 (b) and (d). Summarizing the basic concepts of the geometrical model yields:

- Several m harmonics are needed for describing a ballooned ELM crash
- Harmonics need to be close enough in $q = m/n$ in order to overlap
- Modes minimize n and thereby keep $m = nq$ about constant

In addition to the simple geometric model, simulations of ELM crashes were performed with the JOREK code based on the case described in [41], in which q_{95} was modified by changing the toroidal magnetic field strength while leaving all other parameters unchanged. A clear trend is observed of lower dominant mode numbers at larger q_{95} values, which qualitatively agrees very well with the experimental observations: The dominant mode numbers are $n_{q_{95}=4} = 6 \pm 1$, $n_{q_{95}=5} = 5.5 \pm 1$, $n_{q_{95}=6} = 4 \pm 1$, $n_{q_{95}=8} = 2 \pm 1$. The simulation with $q_{95} = 6$ corresponds to the experimental discharge and the simulations reported in [41]. While the absolute mode number distribution at $q_{95} = 4$ and 5 might be shifted to slightly higher or lower values, because the toroidal resolution used ($n = 0$–8) might be insufficient for these cases, the trend of lower mode numbers for higher q_{95} is very reliable from the JOREK simulations. A detailed analysis of the mechanisms in the simulations in comparison with the simple model is left for future work.

5. Summary

The influence of plasma parameters on toroidal structure as well as duration and losses of the ELM crash was investigated with a database of 30 discharges with more than 2500 ELMs.

The toroidal structure of the ELM crash is strongly influenced by the edge safety factor q_{95}, i.e. higher average toroidal mode numbers $\langle n \rangle$ appear during the crash for lower q and thereby lower ∇q cases. This effect can, however, not be separated from the influence of the pedestal top density which increases $\langle n \rangle$ accordingly. To disentangle both effects future experiments which vary the toroidal magnetic field would be necessary. Nevertheless, nonlinear modeling with JOREK shows the same $\langle n \rangle$ trend with a pure variation of the magnetic field supporting the dominant role of q_{95}. Furthermore, an intuitive qualitative geometrical model was proposed that shows that lower ∇q values need higher toroidal mode numbers in order to have close enough structures for interaction. This sets a lower boundary for the n numbers that are in general minimized during the crash in order to influence a broader region.

Other parameters such as normalized pressure gradient, bootstrap current density or triangularity have a weaker influence on the toroidal geometry. All investigated parameters also influence the n number of low frequency ELM precursors in a very similar way as the n number during the crash. Therefore both phenomena (crash and precursor) appear with similar n.

ELM duration and energy losses are influenced in opposite ways. Higher pedestal energy

results in higher ELM energy losses. On the other hand discharges with higher pedestal energy by trend have higher current and thereby reduced q_{95} values. A reduced q_{95} decreases ELM duration maybe due to reduced ELM penetration depth or reduced ELM structure size (increased n).

Acknowledgment

This work has been carried out within the framework of the EUROfusion Consortium and has received funding from the Euratom research and training programme 2014-2018 under grant agreement No 633053. The views and opinions expressed herein do not necessarily reflect those of the European Commission.
G. F. Harrer is a fellow of the Friedrich Schiedel Foundation for Energy Technology.

References

[1] Zohm H 1996 *Plasma Phys.Control.Fusion* **38** 105–128 ISSN 0741-3335 URL http://stacks.iop.org/0741-3335/38/i=2/a=001
[2] Wilson H 2010 *Fusion Science and Technology* **57** 174–182 URL http://dx.doi.org/10.13182/FST10-A9408
[3] Kirk A, Dunai D, Dunne M, Huijsmans G, Pamela S, Becoulet M, Harrison J, Hillesheim J, Roach C and Saarelma S 2014 *Nuclear Fusion* **54** 114012 URL http://stacks.iop.org/0029-5515/54/i=11/a=114012
[4] Herrmann A, Eich T, Jachmich S, Laux M and Andrew P 2003 *Journal of nuclear materials* **313** 759–767 ISSN 0022-3115 URL http://dx.doi.org/10.1016/S0022-3115(02)01422-8
[5] Loarte A, Saibene G, Sartori R, Eich T, Kallenbach A, Suttrop W, Kempenaars M, Beurskens M, de Baar M, Lnnroth J, Lomas P J, Matthews G, Fundamenski W, Parail V, Becoulet M, Monier-Garbet P, de la Luna E, Gonalves B, Silva C, Corre Y and to the EFDA-JET Workprogramme C 2004 *Physics of Plasmas* **11** 2668–2678 URL http://aip.scitation.org/doi/abs/10.1063/1.1707025
[6] Gohil P, Ali Mahdavi M, Lao L, Burrell K H, Chu M S, DeBoo J C, Hsieh C L, Ohyabu N, Snider R T, Stambaugh R D and Stockdale R E 1988 *Phys. Rev. Lett.* **61**(14) 1603–1606 URL https://link.aps.org/doi/10.1103/PhysRevLett.61.1603
[7] Connor J, Hastie R, Wilson H and Miller R 1998 *Physics of plasmas* **5** 2687–2700 ISSN 1070-664X URL http://scitation.aip.org/content/aip/journal/pop/5/7/10.1063/1.872956
[8] Snyder P B, Groebner R J, Leonard A W, Osborne T H and Wilson H R 2009 *Phys.Plasmas* **16** 056118 URL http://dx.doi.org/10.1063/1.3122146
[9] Krebs I, Hoelzl M, Lackner K and Guenter S 2013 *Physics of plasmas* **20** 082506 ISSN 1070-664X URL http://scitation.aip.org/content/aip/journal/pop/20/8/10.1063/1.4817953
[10] Aydemir A Y 2007 *Physics of Plasmas* **14** 056118 URL https://doi.org/10.1063/1.2727330
[11] Morales J A, Bcoulet M, Garbet X, Orain F, Dif-Pradalier G, Hoelzl M, Pamela S, Huijsmans G T A, Cahyna P, Fil A, Nardon E, Passeron C and Latu G 2016 *Physics of Plasmas* **23** 042513 URL https://doi.org/10.1063/1.4947201
[12] Orain F, Bécoulet M, Huijsmans G T A, Dif-Pradalier G, Hoelzl M, Morales J, Garbet X, Nardon E, Pamela S, Passeron C, Latu G, Fil A and Cahyna P 2015 *Phys. Rev. Lett.* **114**(3) 035001 URL http://link.aps.org/doi/10.1103/PhysRevLett.114.035001
[13] Boom J, Classen I, de Vries P, Eich T, Wolfrum E, Suttrop W, Wenninger R, Donn A, Tobias B, Domier C, Jr N L, Park H and the ASDEX Upgrade Team 2011 *Nuclear Fusion* **51** 103039 URL http://stacks.iop.org/0029-5515/51/i=10/a=103039

[14] Terry J, Cziegler I, Hubbard A, Snipes J, Hughes J, Greenwald M, LaBombard B, Lin Y, Phillips P and Wukitch S 2007 *Journal of Nuclear Materials* **363 - 365** 994 – 999 ISSN 0022-3115 URL http://www.sciencedirect.com/science/article/pii/S0022311507002048

[15] Lee J E, Yun G S, Lee W, Kim M H, Choi M, Lee J, Kim M, Park H K, Bak J G, Ko W H and Park Y S 2017 *Scientific Reports* 45075 URL http://dx.doi.org/10.1038/srep45075

[16] Wenninger R, Reimerdes H, Sauter O and Zohm H 2013 *Nuclear Fusion* **53** 113004 URL http://stacks.iop.org/0029-5515/53/i=11/a=113004

[17] Yu J H, Boedo J A, Hollmann E M, Moyer R A, Rudakov D L and Snyder P B 2008 *Physics of Plasmas* **15** 032504 URL http://dx.doi.org/10.1063/1.2898404

[18] Eich T, Herrmann A, Neuhauser J, Dux R, Fuchs J C, Gnter S, Horton L D, Kallenbach A, Lang P T, Maggi C F, Maraschek M, Rohde V, Schneider W and the ASDEX Upgrade Team 2005 *Plasma Physics and Controlled Fusion* **47** 815 URL http://stacks.iop.org/0741-3335/47/i=6/a=007

[19] Sugiyama L E and the M3D Team 2009 *Journal of Physics: Conference Series* **180** 012060 URL http://stacks.iop.org/1742-6596/180/i=1/a=012060

[20] Sovinec C, Glasser A, Gianakon T, Barnes D, Nebel R, Kruger S, Schnack D, Plimpton S, Tarditi A and Chu M 2004 *Journal of Computational Physics* **195** 355 – 386 ISSN 0021-9991 URL http://www.sciencedirect.com/science/article/pii/S0021999103005369

[21] Huysmans G and Czarny O 2007 *Nuclear Fusion* **47** 659 URL http://stacks.iop.org/0029-5515/47/i=7/a=016

[22] Osborne T, Beurskens M, Horton L, Frassinetti L, Groebner R, Leonard A, Lomas P, Nunes I, Saarelma S, Snyder P, Balboa I, Bray B, Cromb K, Flanagan J, Giroud C, Giovannozzi E, Kempenaars M, Kohen N, Loarte A, Lnnroth J, de la Luna E, Maddison G, Maggi C, McDonard D, McKee G, Pasqualotto P, Saibene G, Sartori R, Solano E, Suttrop W, Wolfrum E, Walsh M, Yan Z, Zabeo L, Zarzosoand D, the JET-EFDA, the DIII-D and the AUG teams 2009 Scaling of the H-mode pedestal and ELM characteristics with gyro-radius on the JET and DIII-D tokamaks *51st APS Meeting of the Division of Plasma Physics Atlanta, Georgia*

[23] Frassinetti L, Dodt D, Beurskens M, Sirinelli A, Boom J, Eich T, Flanagan J, Giroud C, Jachmich M, Kempenaars M, Lomas P, Maddison G, Maggi C, Neu R, Nunes I, von Thun C P, Sieglin B, Stamp M and Contributors J E 2015 *Nuclear Fusion* **55** 023007 URL http://stacks.iop.org/0029-5515/55/i=2/a=023007

[24] Mink F, Wolfrum E, Maraschek M, Zohm H, Horváth L, Laggner F M, Manz P, Viezzer E, Stroth U and the ASDEX Upgrade Team 2016 *Plasma Physics and Controlled Fusion* **58** 125013 URL http://stacks.iop.org/0741-3335/58/i=12/a=125013

[25] Poli F M, Sharapov S E and Contributors J E 2009 *Journal of Plasma and Fusion Research SERIES* **8** 399–403

[26] Mink A F, Hoelzl M, Wolfrum E, Orain F, Dunne M, Lessig A, Pamela S, Manz P, Maraschek M, Huijsmans G, Becoulet M, Laggner F, Cavedon M, Lackner K, Gnter S, Stroth U and Team T A U 2018 *Nuclear Fusion* **58** 026011 URL http://stacks.iop.org/0029-5515/58/i=2/a=026011

[27] Laggner F M, Wolfrum E, Cavedon M, Mink F, Viezzer E, Dunne M G, Manz P, Doerk H, Birkenmeier G, Fischer R, Fietz S, Maraschek M, Willensdorfer M, Aumayr F, the EUROfusion MST1 Team and the ASDEX Upgrade Team 2016 *Plasma Physics and Controlled Fusion* **58** 065005 URL http://stacks.iop.org/0741-3335/58/i=6/a=065005

[28] Maingi R, Bush C, Fredrickson E, Gates D, Kaye S, LeBlanc B, Menard J, Meyer H, Mueller D, Nishino N, Roquemore A, Sabbagh S, Tritz K, Zweben S, Bell M, Bell R, Biewer T, Boedo J, Johnson D, Kaita R, Kugel H, Maqueda R, Munsat T, Raman R, Soukhanovskii V, Stevenson T and Stutman D 2005 *Nuclear Fusion* **45** 1066 URL http://stacks.iop.org/0029-5515/45/i=9/a=006

[29] Sauter O, Angioni C and Lin-Liu Y R 1999 *Physics of Plasmas* **6** 2834–2839 URL https://doi.org/10.1063/1.873240

[30] Freidberg J 1987 *Ideal magnetohydrodynamics* Modern Perspectives in Energy Series (Plenum Publishing Company Limited) ISBN 9780306425127 URL https://books.google.de/books?id=UMDvAAAAMAAJ

[31] Snyder P, Wilson H, Ferron J, Lao L, Leonard A, Mossessian D, Murakami M, Osborne T, Turnbull A and Xu X 2004 *Nuclear Fusion* **44** 320 URL http://stacks.iop.org/0029-5515/44/i=2/a=014

[32] Wilson H R and Miller R L 1999 *Physics of Plasmas* **6** 873–876 URL https://doi.org/10.1063/1.873326

[33] Eich T, Sieglin B, Thornton A, Faitsch M, Kirk A, Herrmann A and Suttrop W 2017 *Nuclear Materials and Energy* **12** 84 – 90 ISSN 2352-1791 proceedings of the 22nd International Conference on Plasma Surface Interactions 2016, 22nd PSI URL http://www.sciencedirect.com/science/article/pii/S2352179116302927

[34] Trier E, Wolfrum E, Willensdorfer M, Yu Q, Ryter F, Angioni C, Dunne M, Denk S, Fischer R, Hennequin P, Kurzan B, Odstrcil T, Schneider P, Stroth U and Vanovac B 2017 Elm-induced cold pulses propagation in asdex upgrade *Proceedings of the 44th EPS Plasma Physics Conference*

[35] Viezzer E, Ptterich T, Angioni C, Bergmann A, Dux R, Fable E, McDermott R, Stroth U, Wolfrum E and the ASDEX Upgrade Team 2014 *Nuclear Fusion* **54** 012003 URL http://stacks.iop.org/0029-5515/54/i=1/a=012003

[36] Sauter P, Ptterich T, Ryter F, Viezzer E, Wolfrum E, Conway G, Fischer R, Kurzan B, McDermott R, Rathgeber S and the ASDEX Upgrade Team 2012 *Nuclear Fusion* **52** 012001 URL http://stacks.iop.org/0029-5515/52/i=1/a=012001

[37] Cavedon M, Ptterich T, Viezzer E, Laggner F M, Burckhart A, Dunne M, Fischer R, Lebschy A, Mink F, Stroth U, Willensdorfer M, Wolfrum E and the ASDEX Upgrade Team 2017 *Plasma Physics and Controlled Fusion* **59** 105007 URL http://stacks.iop.org/0741-3335/59/i=10/a=105007

[38] Hasegawa A, Maclennan C G and Kodama Y 1979 *The Physics of Fluids* **22** 2122–2129 URL http://aip.scitation.org/doi/abs/10.1063/1.862504

[39] Xia H and Shats M G 2003 *Phys. Rev. Lett.* **91**(15) 155001 URL https://link.aps.org/doi/10.1103/PhysRevLett.91.155001

[40] Manz P, Ramisch M and Stroth U 2009 *Plasma Physics and Controlled Fusion* **51** 035008 URL http://stacks.iop.org/0741-3335/51/i=3/a=035008

[41] Hoelzl M, Huijsmans G, Orain F, Artola F, Pamela S, Becoulet M, van Vugt D, Liu F, Futatani S, Lessig A, Wolfrum E, Mink F, Trier E, Dunne M, Viezzer E, Eich T, Vanovac B, Frassinetti L, Guenter S, Lackner K, Krebs I, the ASDEX Upgrade Team and the EUROfusion MST1 Team accepted 2018 *Contributions to Plasma Physics*